Acta Cryst. (1994). B50, 382–395

Symmetry-Modified Conformational Mapping and Classification of the Medium Rings from Crystallographic Data. II. *exo*-Unsaturated and Heterocyclic Seven-Membered Rings

BY FRANK H. ALLEN*

Cambridge Crystallographic Data Centre, 12 Union Road, Cambridge CB2 1EZ, England

JUDITH A. K. HOWARD* AND NIGEL A. PITCHFORD

Department of Chemistry, University of Durham, South Road, Durham DH1 3LE, England

AND J. G. VINTER

University Chemical Laboratory, Lensfield Road, Cambridge CB2 1EW, England

(*Received* 12 *August* 1993; *accepted* 25 *January* 1994)

Abstract

Crystallographic results derived from the Cambridge Structural Database (CSD) have been used to perform a systematic conformational analysis for methylenecycloheptane, oxocycloheptane, azocycloheptane, oxepane, azepane and for the ε-lactone and ε-lactam fragments. Conformational mappings based on symmetry-adapted deformation coordinates and principal component scores show that ring conformations in these fragments fall almost exclusively on the chair–twist-chair pseudorotation pathway. Symmetry-modified Jarvis–Patrick clustering has been used to generate conformational classifications in a semi-automated manner. A manual classification was preferred for the oxocycloheptanes due to wide conformational diversity within a rather small data set. Energy calculations have also been carried out for these systems using force-field methods and a novel conformation-hunting algorithm that attempts to locate all local minima without recourse to ring cleavage and reformation. There is good qualitative agreement between the crystallographic observations of conformation and the calculated features of the potential energy hypersurface, despite the wide variety of substitution patterns covered by the crystallographic results.

Introduction

System analyses of experimental conformational data from crystal structure determinations are of fundamental chemical interest, since it is reasonable to assume that these observations will be closely aligned with the low-energy features of the relevant conformational hypersurface. The aim of this short series of papers is to examine, map and classify the crystallographically observed conformations of the medium alicyclic rings and associated cyclic substructures using the Cambridge Structural Database (CSD; Allen *et al.*, 1991) as the source of experimental results. In part I of this series (Allen, Howard & Pitchford, 1993) we made use of symmetry-adapted deformation coordinates, dissimilarity calculations, principal component analysis and cluster analysis to map and classify the observed conformations of the parent cycloheptane [(I) in Fig. 1]. These methods are now applied to a comparative conformational analysis of a variety of *exo*-unsaturated and heterocyclic analogues of (I) [(II)–(VIII) in Fig. 1], *i.e.* rings which have seven intra-annular single bonds. Wherever possible, the experimental results are related to conformational energy differences obtained from the literature or as calculated here by force-field methods for each individual substructure. A similar analysis of *endo*-unsaturated seven-membered rings is presented in part III (Allen, Garner, Howard & Pitchford, 1994).

Conformational space for seven-membered rings

Conformational space for cycloheptane may be defined by four symmetry-adapted deformation coordinates (hereinafter referred to as BPRS coordinates): ρ, describing the degree of ring pucker; θ, describing the proportion of chair-like or boat-like character of a given ring; and φ_2,φ_3 which describe the degree of twist in a given ring (Pickett & Strauss, 1970; Bocian, Pickett, Rounds & Strauss, 1975; Bocian & Strauss, 1977*a*). The space may also be mapped by the use of the four (related) puckering coordinates of Cremer & Pople (1975), which occur

* Authors for correspondence.

as two amplitude–phase pairs, q_2,φ_2 and q_3,φ_3. These CP coordinates describe two pseudorotational subspaces that map boat (B)–twist-boat (TB) and chair (C)–twist-chair (TC) interconversions, respectively. Conformational diagrams for the symmetric archetypal forms TC(C_2), C(C_s), TB(C_2) and B(C_s) are given as (IX)–(XII). The phase angles φ_2,φ_3 are common to both BPRS and CP descriptions, and Boeyens & Evans (1989) have shown that θ,ρ (BPRS) are related to q_2,q_3 (CP) *via*

$$\rho^2 = q_2^2 + q_3^2 \quad (1)$$

$$\theta = \tan^{-1}(q_3/q_2). \quad (2)$$

Values of intra-annular torsion angles, BPRS and CP coordinates for the symmetrical forms of (I) are given in Table 1.

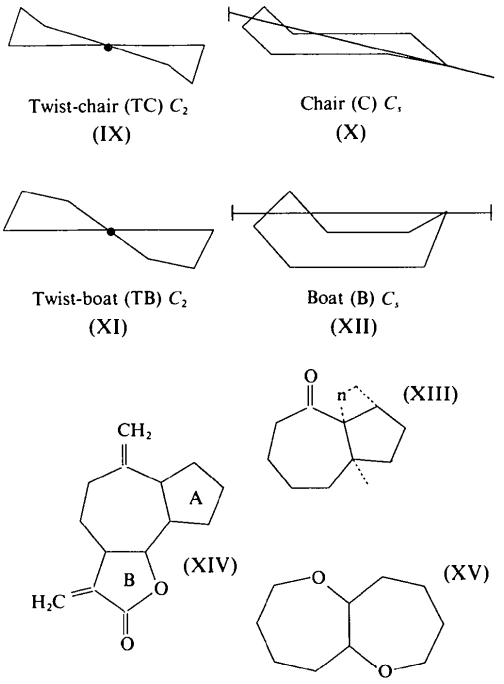

Bocian *et al.* (1975) and Bocian & Strauss (1977*a*) describe the four-dimensional hypersurface in terms of two mutually perpendicular tori. The C–TC pseudorotation follows a helical pathway on a torus of major radial coordinate φ_3 and minor radial coordinate φ_2. All permutational isomers of the C–TC conformers, and their enantiomers, fall on this helical track at $\theta \simeq 50$–$70°$. The B–TB conformers and their equivalents fall on a similar helical track on a torus of the major radial coordinate φ_2 and the minor radial coordinate φ_3. However, since θ tends to zero for the B–TB forms, this pseudorotation itinerary is essentially circular in φ_2. In part I of this series (Allen, Howard & Pitchford, 1993) we showed that: (*a*) the principal component plots derived from a symmetry-expanded torsional data set of 101 cycloheptane fragments are formally equivalent to plots based on the CP coordinates, (*b*) the energetically preferred TC and C conformers dominate the data set (89%), and (*c*) the θ histogram and the φ_2,φ_3 and φ_2,θ scattergrams provide valuable visual overviews of conformational complexity and conformational interconversions.

The φ_2,φ_3 plot is particularly informative for the predominant C/TC conformers, since the helical pathway is dependent on both radial coordinates. For a general asymmetric cycloheptane there exist 28 equivalent conformers arising from the permutational isomers [(I)] and their enantiomers. However, for the C_s- and C_2-symmetric conformers there are only 14 permutations/inversions in each case. If we define the 'origin' chair (C) and twist-chair (TC) conformers at $\varphi_2^o(\mathrm{C}) = 0$, $\varphi_3^o(\mathrm{C}) = \pi$ and $\varphi_2^o(\mathrm{TC}) = \pi/2$, $\varphi_3^o(\mathrm{TC}) = \pi/2$ (Table 1), then permutational isomers (k) will occur (Bocian, Pickett, Rounds & Strauss, 1975; Bocian & Strauss, 1977*a*; Boessenkool & Boeyens, 1980) on the helical track at

$$\varphi_2^k(\mathrm{C,TC}) = \varphi_2^o(\mathrm{C,TC}) + 3\pi k/7;$$
$$\varphi_3^k(\mathrm{C,TC}) = \varphi_3^o(\mathrm{C,TC}) + \pi k/7 \quad \text{for } k = 0\text{–}13, \quad (3)$$

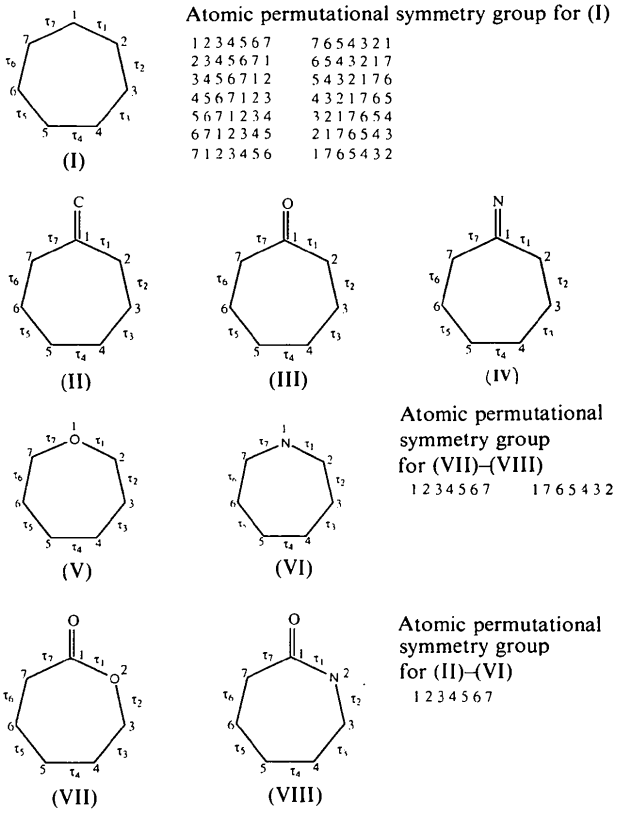

Fig. 1. Substructures studied in this analysis.

Table 1. *Torsion angles (Hendrickson, 1967) for the symmetrical forms TC, C, TB, B [(IX)–(XII)] of cycloheptane* (I)

The symmetry coordinates θ, ρ (Bocian, Pickett, Rounds & Strauss, 1975) and q_2, φ_2; q_3, φ_3 (Cremer & Pople, 1975) are also given together with the conformational designators appropriate for the torsion angles cited.

	Conformation			
Parameter	TC	C	TB	B
τ_1	−39.1	63.8	45.4	−57.5
τ_2	88.1	−83.5	−64.4	−30.9
τ_3	−72.3	66.1	−17.9	69.9
τ_4	54.3	0.0	74.6	0.0
τ_5	−72.3	−66.1	−17.9	−69.9
τ_6	88.1	83.5	−64.4	30.9
τ_7	−39.1	−63.8	45.4	57.5
θ	50	54	≈0	≈0
ρ	0.80	0.74	1.15	1.15
q_2	0.52	0.43	1.15	1.15
φ_2	90.0	0.0	270.0	0.0
q_3	0.61	0.60	0.0	0.0
φ_3	90.0	180.0	--	--
Designator	TC^4	C^4	TB^4	B^4

and the TC conformers occur midway between the C conformers at

$$\varphi_2^k(\mathrm{TC}) = \varphi_2^k(\mathrm{C}) + 3\pi/14;\ \varphi_3^k(\mathrm{TC}) = \varphi_2^k(\mathrm{C}) + \pi/14. \quad (4)$$

For the φ_2-dependent B–TB pathway, and with origin B and TB conformers at $\varphi_2^o(\mathrm{B}) = 0$ and $\varphi_2^o(\mathrm{TB}) = 3\pi/2$ (Table 1), then permutational isomers (k) occur at

$$\varphi_2^k(\mathrm{B,TB}) = \varphi_2^o(\mathrm{B,TB}) + \pi k/7 \quad \text{for } k = 0\text{–}13. \quad (5)$$

The boat-family conformers will overlap with some of the C/TC conformers in a full φ_2,φ_3 map, but the two families can be separated (*a*) by plotting φ_2,φ_3 maps for $\theta \geq 40°$ to isolate the chair-like forms, and (*b*) by plotting a φ_2,θ plot or a φ_2 histogram for $\theta < 40°$ to isolate the boat-like forms.

In part I (Allen, Howard & Pitchford, 1993) we developed a nomenclature for C/TC and for B/TB isomers based upon the position of the unique bond which is bisected by the C_s or C_2 symmetry element. This nomenclature links the φ_2,φ_3 values for a particular isomer to the torsion-angle sequence in the ring. It affords descriptors of the form C^n, TC^n, B^n, TB^n (n = 1–7), where n is the number of the bond (see Table 1) which carries the positive values of the unique torsion angle for the TC, TB(C_2) conformations, and n is the number of the bond that carries the zero torsion angle in the C,B(C_s) conformations. Enantiomeric conformations are then denoted $C^{\bar{n}}$, $TC^{\bar{n}}$, $B^{\bar{n}}$, $TB^{\bar{n}}$. For C,B conformers it is required that τ_{n-1} be positive for C^n, B^n and negative for $C^{\bar{n}}$, $B^{\bar{n}}$. A φ_3 projection of the C/TC pseudorotation itinerary is shown using these descriptors in Fig. 2(*a*); the φ_2-dependent B/TB pathway is illustrated in the radial plot of Fig. 2(*b*). The helical C/TC pathway is, however, best represented by the φ_2,φ_3 plot of Fig. 2(*c*), which also shows an asymmetric unit of this pseudorotational subspace having an area of $\pi^2/7$ rad^2 (1/28 of the area of the complete φ_2,φ_3 map).

For cycloheptane, of course, there is conformational and energetic equivalence between the 14 isomers of each canonical form and there is only one symmetry-independent conformation in each case. It is the low energy barriers between the C and TC forms (*ca* 5–6 kJ mol^{-1}; Burkert & Allinger, 1982) and between the B and TB forms (*ca* 1–2 kJ mol^{-1}; Burkert & Allinger, 1982) that permit pseudorotation. The reduction in topological symmetry from D_{7h} in (I) to C_{2v} in (II)–(VI) gives rise to four possible symmetry-independent conformations in each subclass: C^1–C^4, TC^1–TC^4, B^1–B^4, TB^1–TB^4. This is illustrated in the revised φ_2,φ_3 plot for the C/TC pathway (Fig. 2*d*) in which, for example, C^1 now denotes the symmetry equivalents $C^1 \equiv C^{\bar{1}} \equiv C^7 \equiv C^{\bar{7}}$, and similarly for all C^n and TC^n conformers. The new asymmetric unit marked on Fig.

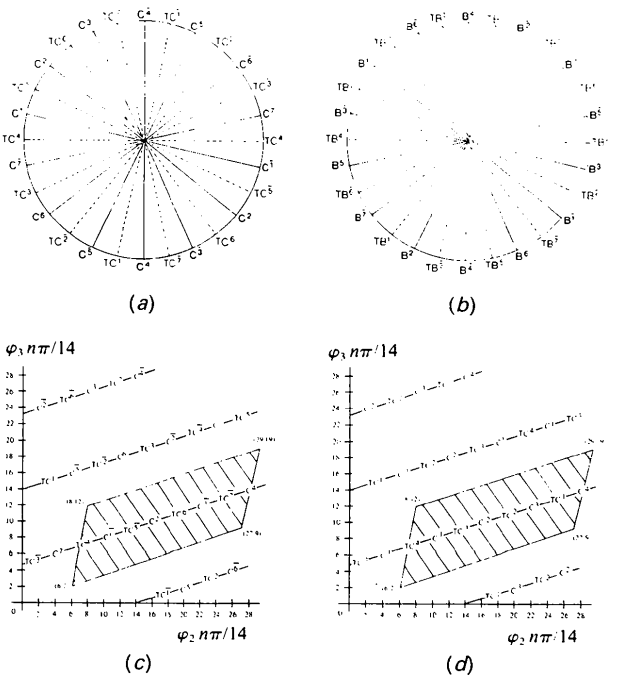

Fig. 2. Idealized conformational mappings for (*a*) chair–twist-chair φ_3-pseudorotation itinerary for cycloheptane. (*b*) boat–twist-boat φ_2-pseudorotation itinerary for cycloheptane, (*c*) $\varphi_2 - \varphi_3$ plot of chair–twist-chair itinerary with a full asymmetric set of conformational descriptors and (*d*) $\varphi_2 - \varphi_3$ plot of chair–twist-chair itinerary with a reduced (C_{2v}) set of conformational descriptors.

2(*d*) now has an area of π^2 rad^2. Each of the symmetry-independent conformers occupies a different energy minimum and pseudorotation can only occur if low-energy barriers exist between the C/TC minima or between the B/TB minima. Fragments (VII) and (VII) are, of course, topologically asymmetric and all seven forms in each canonical subclass are symmetry-independent and energetically unique.

Cycloheptanone (III) has been studied using force-field methods by Allinger, Tribble & Miller (1972) and by Bocian & Strauss (1977*b*). Both papers cite the TC^3 and TC^4 conformations as minimum-energy forms: Allinger *et al.* (1972) calculate TC^4 at 1.05 kJ mol^{-1} higher in energy than TC^3, whilst this difference is almost exactly reversed (0.84 kJ mol^{-1}) by Bocian & Strauss (1977*a*,*b*). These latter authors also calculate the C^1 chair at 0.53 kJ mol^{-1} above TC^4, but find all other C/TC forms at least 6.7 kJ mol^{-1} above the TC^4 minimum. All B/TB forms were calculated at least 9.2 kJ mol^{-1} higher in energy than TC^4, in agreement with the results of Allinger *et al.* (1972). Thus, the C/TC interconversion track has broad low-energy regions encompassing the conformational sequences TC^3–C^1—TC^4—C^1–TC^3 (Fig. 2*d*) bounded by high-energy barriers $\geq$6.7 kJ mol^{-1} along that track and is separated from the boat forms by even higher barriers. To our knowledge no similar force-field calculations have been carried out for the methylene (II) or azo (IV) analogues of cycloheptanone (III).

Vibrational spectra, and force-field calculations for oxacycloheptane [oxepane (V)] have been presented by Bocian & Strauss (1977*a*,*c*). The calculations predict isolated energy minima for the TC^2 and the TC^3 conformations, with TC^3 preferred by only 0.05 kJ mol^{-1}. All other C/TC conformers are at least 8.1 kJ mol^{-1} above TC^3 and all B/TB forms are at least 10.4 kJ mol^{-1} above the global TC^3 minimum. Similar calculations for azacycloheptane (VI) could not be located.

The conformations of 5,5-difluoro-ε-caprolactone and of its lactam analogue [using the numbering scheme of (VII) and (VIII)] have been investigated by ^{19}F NMR (Noe & Roberts, 1971). These authors show that the barrier to ring inversion in (VII) and (VIII) is high at 42.0 and 43.7 kJ mol^{-1}, respectively, and that the NMR data are best interpreted in terms of a chair conformation in both cases. These results are supported by force-field calculations for the lactone (VII) (Allinger, 1982) which located four energy minima. The global minimum is a C^1 chair conformation with the B^1 boat occupying a local minimum 11.4 kJ mol^{-1} above the chair form. Two other asymmetric intermediate conformations, described as half-chair and *trans*-forms, are 17.8 and 22.3 kJ mol^{-1} higher in energy than the chair form, respectively.

Database methodology

Version 4.6 (January 1992) of the Cambridge Structural Database System was used throughout for substructure search, coordinate retrieval and data analysis, using the programs *QUEST* and *GSTAT* (Allen *et al.*, 1991).

Substructure search

Two general substructure searches were carried out initially in order to assess the chemical variety of seven-membered rings available in the CSD: (i) for a seven-membered ring of atoms *X* connected by single bonds, where *X* = any non-H atom, and (ii) for this same substructure in which one of the atoms carries an *exo* double bond. These searches were further constrained using the CSD bit-screen mechanism (Cambridge Structural Database, 1992) to locate entries with (*a*) atomic coordinates available, (*b*) no residual numerical errors following CSD evaluation procedures, (*c*) no reported disorder in the crystal structure, (*d*) a crystallographic $R \leq 0.12$, (*e*) classified as an 'organic' compound according to the CSD definitions and (*f*) contained no bridged or highly complex ring systems (SCREEN −620 −622), as described in part I (Allen, Howard & Pitchford, 1993). As a result of these general searches, fragments (II)–(VIII) were selected as chemically coherent subsets for further conformational analysis. Individual searches for the selected fragments had C_{sp^2} atoms as identified in Fig. 1, with all other C atoms as sp^3 hybrids. Search results, in terms of the numbers of CSD entries retrieved, the numbers of fragments located and the maximum *R* factor in each data set, are reported in Table 2. The CSD reference codes for all entries used in this study are reported in Table 3 and full literature citations have been deposited.*

Data analysis

The program *GSTAT* (Murray-Rust & Raftery, 1985*a*,*b*; Allen *et al.*, 1991) was used for the calculation and analysis of geometrical parameters and the procedures used here are similar to those employed in part I (Allen, Howard & Pitchford, 1993). The following parameters were generated for all located fragments using the atom and bond enumerations indicated for (II)–(VIII) in Fig. 1: the intra-annular torsion angles τ_1–τ_7; Cremer–Pople (Cremer & Pople, 1975) puckering parameters q_2,φ_2,q_3,φ_3;

* Full literature citations for all CSD entries used in this study have been deposited with the British Library Document Supply Centre as Supplementary Publication No. SUP 71754 (12 pp.). Copies may be obtained through The Managing Editor, International Union of Crystallography, 5 Abbey Square, Chester CH1 2HU, England.

Table 2. *Search results for substructures* (II)–(VIII) (*Fig.* 1)

N_e is the number of CSD entries retrieved, N_f is the number of chemically independent fragments located in those entries and R_{max} is the maximum R factor in each data set. Also included here are the Jarvis–Patrick clustering criteria n, K_{NN}, K_{JP} and D_{max} described in the text, used to generate the results of Table 6(*a*).

	Search results			Jarvis–Patrick criteria			
Substructure	N_e	N_f	R_{max}	n	K_{NN}	K_{JP}	D_{max}
(II)	56	64	0.095	2	10	5	0.08
(III)	30	32	0.096	1	5	3	0.08
(IV)	15	16	0.091	1	5	3	0.08
(V)	33	50	0.103	2	7	3	0.08
(VI)	22	26	0.110	2	5	3	0.08
(VII)	10	10	0.096	2	5	3	0.08
(VIII)	16	23	0.096	1	8	4	0.10

values of θ, ρ (Bocian *et al.*, 1975) calculated from (1) and (2) *via* the TRAnsform command in *GSTAT*. The Cartesian equivalents of the Cremer–Pople (1975) coordinates were also calculated as CP1 = $q_3 \sin \varphi_3$, CP2 = $q_3 \cos \varphi_3$ (mapping C/TC conformers) and CP3 = $q_2 \sin \varphi_2$, CP4 = $q_2 \cos \varphi_2$ (mapping B/TB conformers). For the generation of conformational maps, the raw data sets were expanded to fill the conformational space by use of the atomic permutational symmetry operators (Fig. 1) and the inversion operator to yield four permutational isomers per fragment for (II)–(VI) and two isomers for (VII) and (VIII).

Conformational classifications were carried out using the Jarvis–Patrick (1973) algorithm as modified by Allen, Doyle & Taylor (1991*a*) to take account of the effects of permutational isomerism on the intra-annular torsion angles τ_1–τ_7. This procedure, fully described by Allen, Doyle & Taylor (1991*a*) and by Allen, Howard & Pitchford (1993), employs four user-defined variables in each clustering experiment: (i) a power factor (n) defining the metric to be used in torsional dissimilarity calculations, where $n = 1$ for the City-Block metric and $n = 2$ for the Euclidian metric; (ii) K_{NN}, the maximum length of the Jarvis–Patrick nearest-neighbour list for each fragment (p), *i.e.* the number of fragments (q) that are considered to be 'closest' to fragment p; (iii) K_{JP}, the Jarvis–Patrick clustering criterion, *i.e.* the number of fragments (q) that must be common to the nearest-neighbour lists of fragments p_1 and p_2 so that both fragments may be assigned to the same cluster; (iv) D_{max} (a maximum dissimilarity), if $D_{ij} > D_{max}$ then fragment q cannot enter the nearest-neighbour list of fragment p, even if K_{NN} is not yet satisfied. Application of the Jarvis–Patrick (Jarvis & Patrick, 1973) method in conformational classification is still novel, and guidelines as to the most appropriate settings of n, K_{NN} and K_{JP} is valuable. The settings used for the relatively small data sets encountered in this study are also collected in Table 2.

Table 3. *CSD reference codes for structures used in this analysis*

Methylenecycloheptanes (II)

ACHOLB	CELPIS	FAWLUK	SALREC
AIBFOR10	CELPOY	FEBXUF	MIKTIN
BETDOT	CENSIN01	FEJHOR	SANGOD
BGIGAC	CENSIN10	FEMYAX	SAYZOH
BISJUI	CEWRUR10	FIJZED	SERRAT10
BTMUNE	CHSPOX	FOYMEL	SOLSIN
BUMPII	CIDYOD	GAYFOB	TBCMUN
BUVPEN	CODSUJ10	GRLCTN	THIELN10
BUWSAN	CUNPIK	HGUDOL	VENPOT
BUWSAN01	CUPCIZ	HIMCHC	VEPXIX
CARGIL	DAJKOO	HNANDB	XANTHB
CAWGIQ	DANETN	HYPOCH	
CAWGIQ01	DAPTIX	ITNGRO	
CELPAK	DHYGUA	JIDKUC	
CELPEO	DIPXOP	KEJNUI	

Cycloheptanones (III)

APORON	DINMUI10	FOLKUM	HONGUA
BISYUX	DOTJOL	FONFAP	JAMFOS
BOXXOB	FECHEA	FUFLAT	JIDHUZ
CAYZIL	FEGSOZ	FUSNEM	JILJIX
CIYMUD	FEYCER	FUSPAK	LASROL
CIJNAK	FEYREG	GEBRAG	SADYEB
CURFAW	FIKDOS	GETNAU	
DAFCOC	FIXMUU	HAESTD	

Azocycloheptanes (IV)

BOCBEA	BUVVAP	CACBEN	DOTJUR
BOCBIE	BUVVET	CENMIR	DOTKAY
BPAZBH	CABZUA	DORJUP	KANDOS
BPAZTS	CACBAJ	DORKAW	

Oxacycloheptanes (V)

ACGLSP	BUNSIM11	JAMVOI	KEVSEJ
AHIDIT	CIHDIG	JAMVOI10	MAGSEP10
AIPGLC	EIPGLU10	JAMVUI	MIPGSP
AIPMGH	FAJMOS	JAMVUI10	MPASEP
BATLAJ	FISHAQ	JAPGAI	SEVKIN
BERFAF	FISHAQ10	JAPGEM	VEZKAM
BUFFOX	GETKEV	KETVUA	
BUJRED	GETKEV10	KETXUC	
BUJXIN	GLUSPT10	KEVBAO	

Azacycloheptanes (VI)

AZBQUB	CABCUD01	JEBTEP	VUZDID
BACMEC10	CAVFOU	JIDBAZ	XIMBZA
BHAUST	CROOMI	KAVLIC	XIMBZB
BUCXAY	FECYIV	MECILN	XIMBZB01
BUFPEX	FOZKUA	STEMON10	
CABCUD	HEXAMC	VANRAD	

ε-Lactones (VII)

AXHNOM	FAWLEU	JOCCUZ	VESVIY
BEBSIK	JOCCIN	JOCDIO	
BRASSA01	JOCCOT	PRIEUB10	

ε-Lactams (VIII)

BAJZOB10	CAPRES	FEFSUE	VAXYOI
BILJOV	*CAZCHI*	*FULMUU*	*VENTEN*
CAPLAC	DIKVAU	FULNAB	VENTIR
CAPLAC01	DOKMUL	FULNEF	VIMXIY

Energy calculations

The principal aim of the database analysis reported here is to classify the crystallographic observations of (II)–(VIII) into conformational subgroups so as to gain insight into the features of the conformational energy hypersurface. As in part I (Allen, Howard &

Pitchford, 1993), it is useful to correlate these experimental results with details of the energy hypersurface obtained, for example, by force-field or *ab initio* calculations. With the exception of (III), (V) and (VII), we were unable to locate detailed literature reports of such calculations, hence we begin this paper by reporting and discussing the results of a systematic conformational analysis of (II)–(VI) using a consistent force-field approach.

Computational procedures

Software to gather and analyse the accessible conformations of medium rings was based on the philosophy of the *COSMIC* molecular modelling package (Vinter, Davis & Saunders, 1987) and extensions embodied in *COSMIC*90, which incorporates an updated force field for hydrocarbons and conjugated systems (Morley, Abraham, Haworth, Jackson, Saunders & Vinter, 1991). The ring conformation hunter attempts to find all local energy minima without the need to first break and then reform the ring. Ring systems are little influenced by Coulombic forces in this instance and partial charges have been ignored. The user can define the number of randomly generated starting conformations, the total number of conformations to be held during a run and also the energy range within which this number of conformations must lie. The complete procedure is summarized in flow-chart form in Fig. 3. The final output conformations can be viewed and analysed using separate graphical modules.

Results and discussion

Calculated energies (E, kJ mol^{-1}), and energy differences (ΔE) from the relevant global minimum, are reported in Table 4. Literature data for cycloheptanone [(III); Bocian & Strauss, 1977(*b*); Allinger, Tribble & Miller, 1972] and for oxepane [(V); Bocian & Strauss, 1977*a*,*c*] are also included for comparison. The general features of the energy hypersurface for the *exo*-unsaturated (II)–(IV) are very similar: a broad minimum encompasses the TC^3–C$_1$–TC^4 areas of the pseudorotation itinerary (Fig. 2*d*), with symmetry-equivalent minima separated by an energy barrier of *ca* 13–14 kJ mol^{-1}. There exist, however, minor differences between the energy levels of the individual TC^3, C^1 and TC^4 minima, both between substructures and, for (III), between the different calculational methods (each of which employed a different force field). Thus, our calculations consistently yield an energy ordering of TC^3 > TC^4 > C^1, but Bocian & Strauss (1977*b*) indicate a TC^4 global minimum in contrast to the TC^3 minimum of Allinger, Tribble & Miller (1972). However, these fluctuations are probably not predictive since they only span energy variations at the 2.4 kJ mol^{-1} level.

Our results for the hetero-rings (V) and (VI) are again consistent in predicting a TC^3 global minimum in agreement with results of Bocian & Strauss (1977*a*,*c*) for (V). However, their calculations then indicate an almost isoenergetic TC^2 form separated from TC^3 by a C^2 energy barrier of 8.14 kJ mol^{-1} with other conformers of (V) being at higher energies. Our results for (V) and (VI) suggest TC^3 as a clear global minimum, but with much lower energy barriers between TC^3 and other conformers than those predicted by Bocian & Strauss (1977*a*,*c*).

Energy calculations for the lactone [(VII)] have been reported by Allinger (1982). They indicate a dominant C^1 conformer which lies 11.34 kJ mol^{-1} below the next local minimum (a boat conformation). The presence of a single chair conformer for both (VII) and the lactam (VIII) is also indicated by NMR results (Noe & Roberts, 1971).

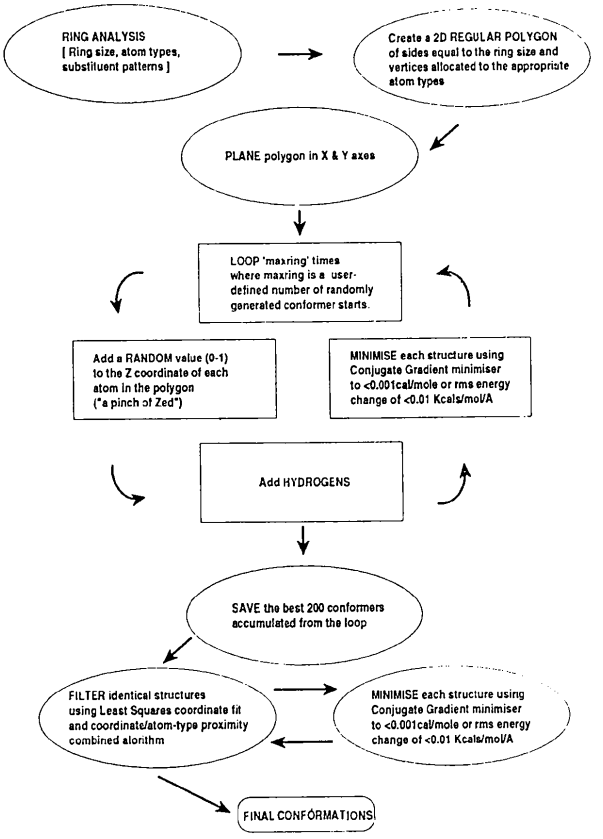

Fig. 3. The conformation hunter, *PCRNGMIN*, and the graphical analysers, *PCAST* and *PCDRAW*, written in FORTRAN77 running under the Salford FTN77 memory manager (Polyhedron Software, 1993) on a PC486 clone with 8 Mb memory. Graphics are generated *via* the INTERACTER VGA PC interface library (Polyhedron Software, 1993). Software also operates on a Silicon Graphics Indigo basic system with 16 Mb memory.

Table 4. *Calculated energies* (E, kJ mol^{-1}) *and values of* ΔE *(the energy difference from the relevant global minimum) for substructures* (II)–(VI)

Literature values are cited where available.

Data set	Function	C^1	C^2	C^3	C^4	TC^1	TC^2	TC^3	TC^4
(II)	E	15.62	24.50	27.00	28.99	23.55	23.09	16.86	16.83
	ΔE	0.00	8.88	11.38	13.37	7.93	7.47	1.24	1.21
(III)	E	12.64	22.62	25.02	26.30	20.71	21.57	15.04	13.09
	ΔE	0.00	9.98	12.38	13.66	8.07	8.93	2.40	0.45
	ΔE^a	0.54	10.56	12.45	13.50	8.39	6.72	0.84	0.00
	ΔE^b					6.80	7.56	0.00	1.05
(IV)	E	8.03	17.62	19.52	22.29	16.62	15.91	10.22	9.75
	ΔE	0.00	9.59	11.49	14.26	8.59	7.88	2.19	1.72
(V)	E	44.01	38.47	40.42	39.44	36.43	37.49	33.85	40.71
	ΔE	10.16	4.62	6.57	5.59	2.58	3.64	0.00	6.86
	ΔE^c	(12.68)	8.14	(11.00)	(16.45)	(8.90)	0.05	0.00	(11.42)
(VI)	E	31.87	32.30	35.65	36.45	32.33	31.44	28.04	31.68
	ΔE	3.83	4.26	7.61	8.41	4.29	3.40	0.00	3.64

References: (*a*) Bocian & Strauss (1977*b*); (*b*) Allinger, Tribble & Miller (1972); (*c*) Bocian & Strauss (1977*a*).

Conformational mapping

BPRS coordinate plots

The conformational diversity of the crystallographic observations of (II)–(VIII) was initially explored using histograms of the BPRS θ-coordinate (Figs. 4*a*–4*g*) and the φ_2,φ_3 scatterplots of Figs. 5(*a*)–5(*g*). Histograms for (II)–(VI) are generated from symmetry-expanded data sets, hence the numbers in each angular bin of Figs. 4(*a*)–4(*e*) represent isomers/enantiomers, *i.e.* four times the number of fragments. Histograms for (VII) and (VIII) (Figs. 4*f* and 4*g*) are generated from raw data sets. The histograms show that C/TC forms, taken as having $\theta \geq 40°$, are dominant for all of the substructures: Table 5 shows that the percentage of C/TC forms is always in excess of 80% using the $\theta \geq 40°$ criterion.

The φ_2,φ_3 scatterplots of Figs. 5(*a*)–5(*g*) are all generated using symmetry expansion for those fragments having $\theta \geq 40°$. The complete C/TC pseudorotation itinerary is exemplified for (II) in Fig. 5(*a*1), but other plots for (II)–(VI) show only the asymmetric unit. Complete maps are shown for (VII) and (VIII). The φ_2,φ_3 plots for (II)–(IV) all show high density in the TC^3–C^1–TC^4 area, as predicted by the energy calculations (Table 4). However, methylenecycloheptane (II) and, to a lesser estent, cycloheptanone (III), both show density in the TC^2 area. TC^4 conformers appear to be absent for (IV). The heterocyclic fragments (V) and (VI) show rather different φ_2,φ_3 patterns. For oxepanes (V), the TC^4 and C^1 conformers are not represented, as suggested by the energy calculations (Table 4). The C^4 conformer is also absent but C^3, one of the higher energy conformers, shows a small population density. The azepanes (VI) show a broad conformational distribution, perhaps a reflection of the rather similar ΔE values (Table 4) for six of the possible symmetric conformers. One of the two higher energy forms (C^4) is also present. The lactones (VII) and lactams (VIII) are predominantly C^1 conformers, as expected.

Principal component analysis (PCA)

Principal component analysis (see *e.g.* Murray-Rust & Bland, 1978; Chatfield & Collins, 1980) was applied to symmetry-expanded torsional data sets for (II)–(VIII) and the results treated in a manner analogous to those for the parent cycloheptane (Allen, Howard & Pitchford, 1993). Here, four non-degenerate principal components (PC's) were found to account for >99.9% of variance in each of the data sets (see Table 5). The symmetry of the PC loadings indicated that each PC mapped one of the symmetric conformations and the percentage of the total variance accounted for by each PC is listed in Table 5.

These results represent a quantification of the visual interpretaton of Figs. 4 and 5 and can also be correlated with the energy calculations of Table 4. Obviously, the C/TC conformations dominate all data sets and the variance ratios C + TC/B + TB, given as %C/TC in Table 5, closely mimic the $\%\theta_h$ values deduced from Fig. 4. For the *exo*-unsaturated rings (II)–(IV), the TC^5, C^1 and TC^4 conformers are of approximately equal (minimum) energy and, in any random sample of rings, we might expect a TC:C ratio of 2:1. The TC:C variance ratios for (II)–(IV) (Table 5) are very close to this value. The very high C:TC ratios for (VII) and (VIII) are also to be expected energetically and are a restatement of Figs. 5(*f*) and 5(*g*) in numerical terms. The energy values of Table 4 would suggest TC:C ratios >1.0 for the hetero-rings (V) and (VI), since TC energies are at a generally lower level than C energies. This is evident from the TC:C variances of Table 5, but the correlation is less convincing than for the other substructures.

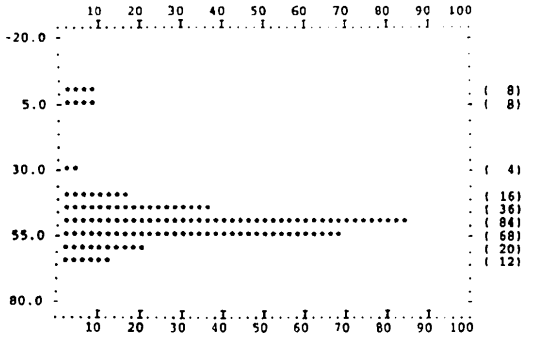

Methylenecycloheptanes (II)
(*a*)

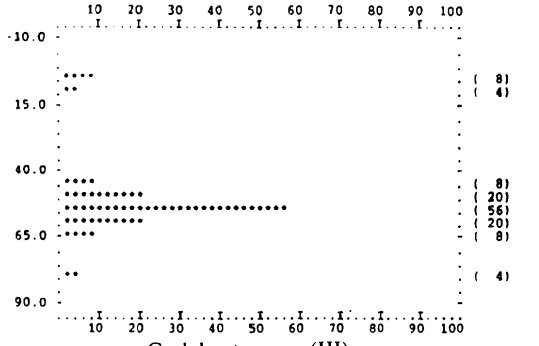

Cycloheptanones (III)
(*b*)

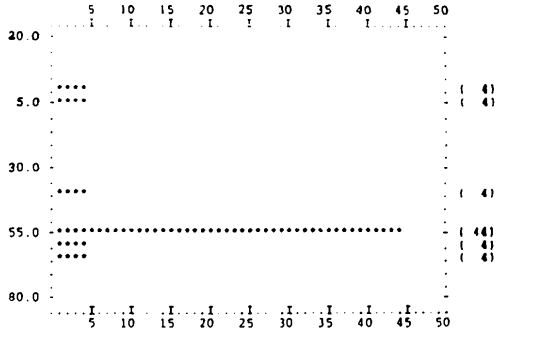

Azocycloheptanes (IV)
(*c*)

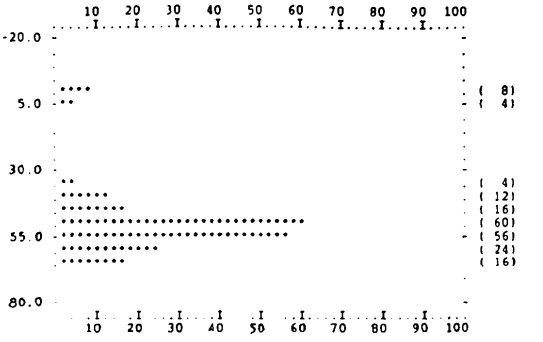

Oxepanes (V)
(*d*)

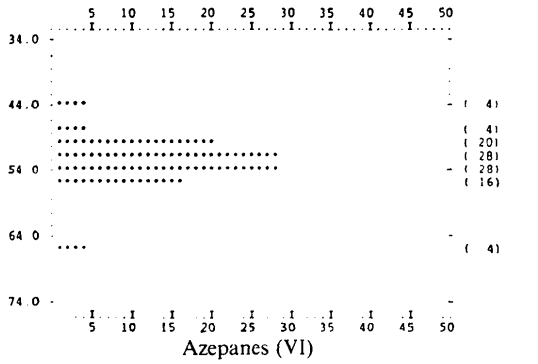

Azepanes (VI)
(*e*)

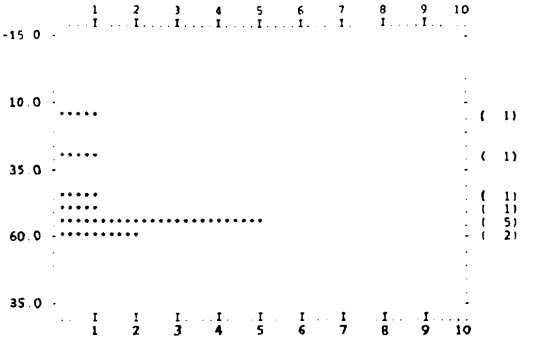

Lactones (VII)
(*f*)

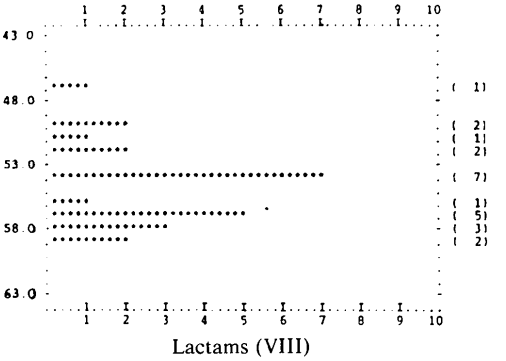

Lactams (VIII)
(*e*)

Fig. 4. θ-histograms for substructures (II)–(VIII).

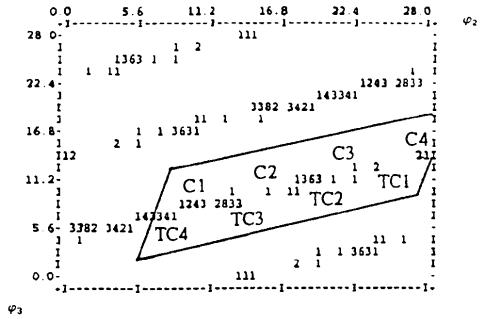

Methylenecycloheptanes (II)
(*a*1)

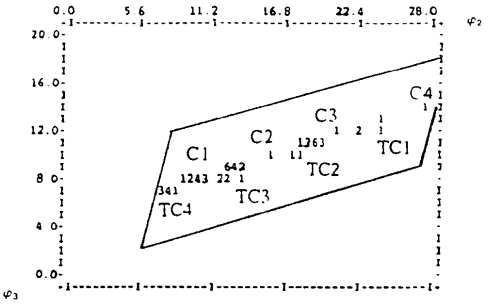

Methylenecycloheptanes (II)
(*a*2)

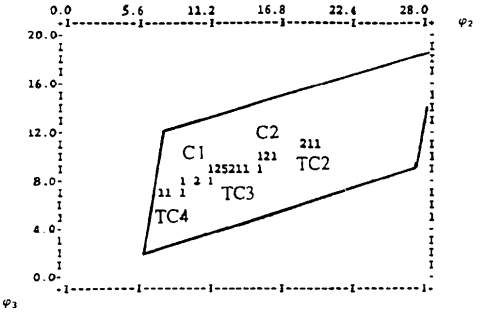

Cycloheptanones (III)
(*b*)

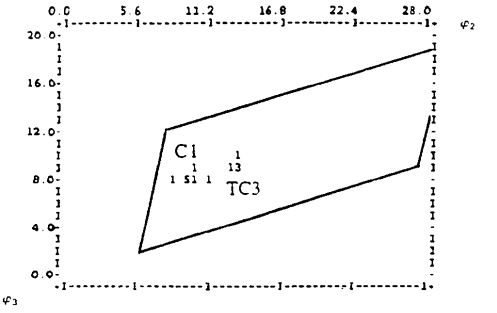

Azocycloheptanes (IV)
(*c*)

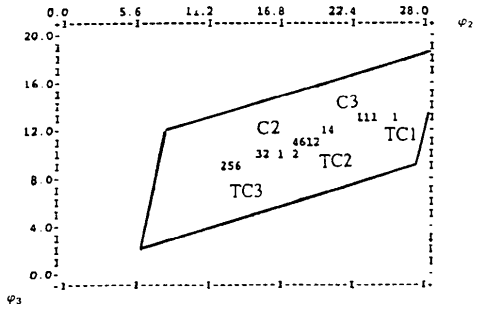

Oxepanes (V)
(*d*)

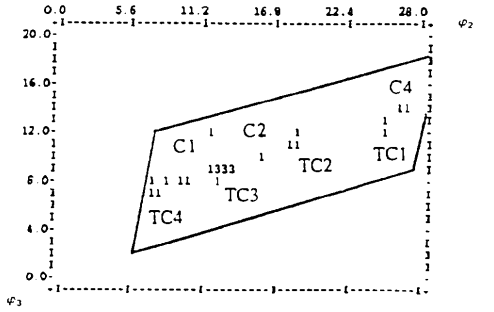

Azepanes (VI)
(*e*)

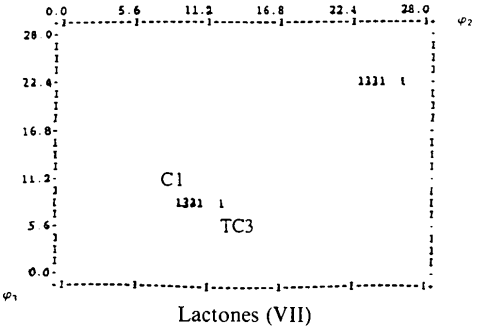

Lactones (VII)
(*f*)

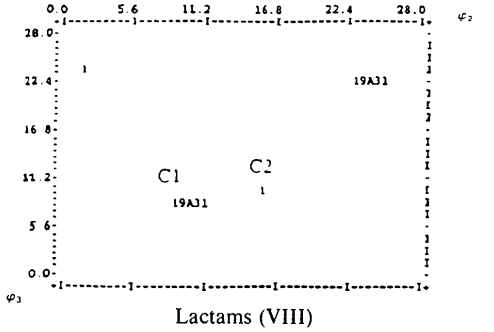

Lactams (VIII)
(*g*)

Fig. 5. $\varphi_2 - \varphi_3$ plots for substructures (II)–(VIII). Part (*a*1) shows all fragments for (II); parts (*a*2) to (*e*) include only those fragments with $\theta \geq 40^\circ$.

Table 5. *Symmetry assignments (TC, C, TB, B) and percentage variance accounted for by each of the four principal components obtained for substructures (II)–(VIII)*

The percentage of variance associated with C, TC conformations (%C/TC) is compared with $\%\theta_n$, the percentage of conformers having a BPRS θ value greater than 40°.

Fragment	TC	C	TB	B	%C/TC	$\%\theta_n$
(II)	54.7	30.4	8.6	6.2	85.1	92.2
(III)	60.5	29.5	5.3	4.7	90.0	90.6
(IV)	69.5	23.3	4.2	2.9	92.8	87.5
(V)	45.6	42.1	5.5	6.8	87.7	86.0
(VI)	59.1	31.3	3.2	6.4	90.4	100
(VII)	5.7	75.1	2.5	16.6	78.8	81.8
(VIII)	2.1	74.1	19.4	4.5	76.2	100

The six PC scatterplots were each prepared for (II)–(VII), as described by Allen, Howard & Pitchford (1993), but only two of these 42 plots are shown in Figs. 6(*a*) and 6(*b*). The PC1 *versus* PC2 plots for the hetero-rings (V) (Fig. 6*a*) and (VI) (Fig. 6*b*) both show a perpendicular, hence circular, view of the C/TC toroidal pseudorotation itinerary [these plots should be compared with those for the parent cycloheptane in Allen, Howard & Pitchford (1993)]. A comparison of Fig. 6(*a*) with Fig. 2(*a*) shows clearly the absence of density in the C^1–TC^4 and C^4 areas and maximum density in the TC^2–C^2–TC^3 areas (see also Fig. 5*d*). The central density in Fig. 6(*a*) represents three B/TB conformers. Since five oxepanes had $\theta < 40°$ (Fig. 4*d*, Table 5), it would appear that $\theta < 25$–$30°$ might have been a more appropriate discriminator of B/TB conformations. In Fig. 6(*b*) we see a more complete distribution of conformations along the C/TC itinerary and the complete absence of B/TB conformers in agreement with the BPRS analysis of Figs. 4(*e*) and 5(*e*).

Conformational classification

Overview

The results of the symmetry-modified Jarvis–Patrick clustering algorithm applied to the torsional data sets (τ_1–τ_7) for substructures (II)–(VIII) are summarized in Table 6(*a*), in the form of mean torsion angles for each cluster having a population (N_p) ≥ 2 fragments. The appropriate conformational descriptor (Fig. 2*d*) is assigned in each case. For the smaller data sets, all except (II) (64 fragments) and (V) (50 fragments), a number of variations in the clustering criteria K_{NN} and K_{JP} (Table 2) were required to generate a chemically acceptable automated classification.

For cycloheptanone (III), however, none of the clustering algorithms described earlier (Allen, Doyle & Taylor, 1991*b*) were able to generate entirely satisfactory results. Close examination of various Jarvis–Patrick runs showed that small twist deformations in the C^1 examples towards both TC^3 and TC^4 conformations were preventing the formation of discrete clusters in automated processes. For this reason, the manual results of Table 6(*b*) are to be preferred for (III). This data set is now being used to test algorithmic modifications designed to reduce these problems.

Despite these difficulties, the results are again instructive in terms of the choice of Jarvis–Patrick

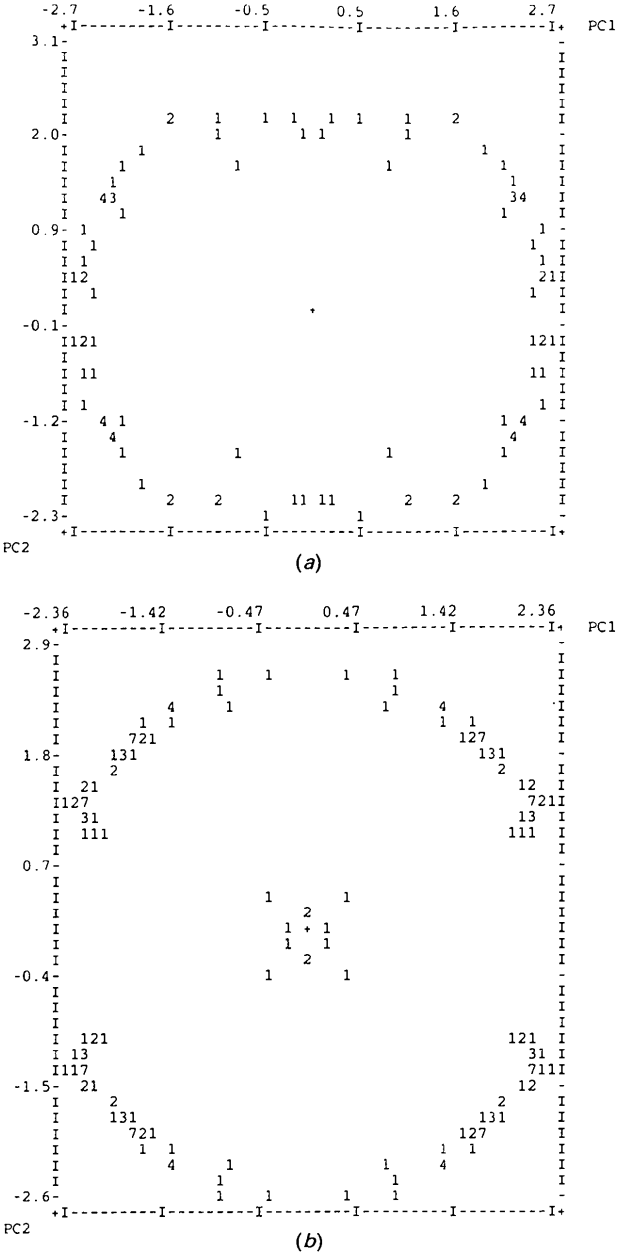

Fig. 6. Scatter plots of principal component scores referred to the PC1, PC2 axes for (*a*) fragment (V) and (*b*) fragment (VI).

Table 6. *Jarvis–Patrick cluster analysis results for the seven data sets and conformational groupings and populations for data set* (III) *by visual assessment*

The mean torsion angles (°) for each cluster are given in (*a*) together with the e.s.d. of each mean (in parentheses) and the CSD refcode of the most representative fragment in that particular cluster. The torsion angles in (*b*) are those of a characteristic example of each conformation.

(*a*) Jarvis–Patrick cluster analysis

Fragment	Conformation	N_p	M.r.f.	τ_1	τ_2	τ_3	τ_4	τ_5	τ_6	τ_7
(II)	TC^3	15	DHYGUA	−86.0 (17)	70.2 (14)	−52.7 (14)	71.0 (11)	−88.4 (11)	43.2 (15)	35.3 (7)
	TC^2	14	SAYZOH	−67.6 (20)	42.9 (25)	−65.5 (13)	94.1 (13)	−45.8 (12)	−35.1 (12)	88.4 (7)
	C^1	12	MIKTIN	0.9 (15)	64.6 (13)	−84.9 (8)	64.5 (15)	−62.0 (10)	77.8 (14)	−62.8 (17)
	TC^4	8	CELPEO	−28.5 (16)	81.7 (17)	−74.9 (14)	56.0 (17)	−68.6 (21)	85.4 (15)	−45.7 (17)
	C^2	2		69.5 (13)	−10.4 (0)	−57.2 (4)	88.4 (20)	−71.2 (27)	59.3 (26)	−75.1 (16)
(III)	C^1/TC^3	4	HONGUA	19.7 (33)	−81.3 (9)	82.5 (26)	−61.2 (17)	65.9 (11)	−85.4 (8)	55.1 (24)
	TC^3	4	JILJIX	−84.2 (15)	75.1 (12)	−59.6 (19)	70.0 (13)	−79.8 (21)	39.2 (19)	33.7 (10)
	TC^3	4	DOTJOL	−97.4 (21)	69.0 (9)	−54.6 (10)	76.2 (9)	−85.2 (15)	28.7 (30)	52.8 (24)
	C^1/TC^4	3		−18.5 (57)	−48.0 (44)	77.6 (18)	−65.6 (17)	61.5 (10)	−79.5 (8)	74.6 (40)
	C^2	3		−63.8 (20)	0.3 (37)	70.9 (79)	−90.5 (65)	62.4 (28)	−62.4 (26)	83.2 (1)
(IV)	C^1	8	BUVVAP	1.3 (21)	64.2 (24)	−84.6 (29)	65.6 (13)	−62.4 (14)	80.8 (14)	−65.9 (11)
	TC^3	5	CACBEN	94.6 (10)	−70.7 (8)	57.2 (11)	−74.8 (4)	79.4 (13)	−25.8 (14)	−51.7 (8)
(V)	TC^3	17	BUJRED	−98.9 (7)	67.1 (17)	−46.6 (21)	67.1 (10)	−84.3 (14)	32.9 (11)	52.8 (9)
	TC^2	12	JAMVUI	−82.7 (6)	54.9 (11)	−67.5 (11)	86.3 (9)	−43.9 (13)	−33.1 (12)	94.0 (9)
	C^2	8	GETKEV	−59.2 (41)	−3.5 (41)	73.6 (18)	−90.3 (21)	63.7 (7)	−63.8 (20)	79.1 (14)
	C^3	5	JAMVOI	−75.7 (13)	74.2 (7)	−15.1 (17)	−58.6 (6)	100.3 (6)	−78.6 (4)	59.8 (15)
(VI)	TC^3	11	VANRAD	86.8 (15)	−71.8 (16)	53.8 (14)	−68.3 (7)	87.0 (16)	−43.4 (27)	−36.3 (26)
	C^1/TC^4	6	STEMON10	14.7 (42)	55.5 (36)	−86.3 (18)	65.9 (18)	−56.1 (18)	76.7 (24)	−72.7 (24)
(VII)	C^1	8	JOCCOT	−0.9 (23)	64.5 (20)	−77.1 (17)	59.1 (14)	−58.8 (14)	79.8 (13)	−66.4 (20)
(VIII)	C^1	23	CAPLAC01	−2.1 (8)	68.1 (9)	−78.2 (5)	59.5 (8)	−61.3 (8)	81.2 (9)	−65.1 (8)

(*b*) Conformational groupings and populations for data set (III)

Fragment	Conformation	N_f	Refcode	τ_1	τ_2	τ_3	τ_4	τ_5	τ_6	τ_7
(III)	TC^3	12	FUSNEM	87.0	−74.9	58.1	−68.3	82.8	−41.1	−36.5
(III)	C^1	5	JIDHUZ	1.4	−59.0	83.4	−74.7	68.4	−67.5	51.3
(III)	C^2	5	HAESTD	−72.5	5.8	59.8	−82.9	64.4	−64.2	88.4
(III)	TC^2	4	FUFLAT	−80.8	52.1	−68.2	86.1	−40.2	−36.1	95.0

criteria K_{NN} and K_{JP}. Earlier experiences (Allen, Doyle & Taylor, 1991*a*,*b*; Allen, Howard & Pitchford, 1993) indicated that a K_{JP}/K_{NN} ratio close to 0.5 was effective in generating clusters that conformed to the more subjective, but most important, criterion of chemical sensibility. These observations are reinforced by the K_{JP}/K_{NN} ratios of Table 2 which vary from 0.43 to 0.60 for a series of small integer values.

In our implementation, the Jarvis–Patrick software automatically identifies the most representative fragment (m.r.f.) in each cluster, *i.e.* the fragment which is closest to the cluster centroid. Indeed, it is individual torsion angles from these entries that are used to illustrate the manual classification of Table 6(*b*), except for (III) where m.r.f.'s have been manually assigned. We report orthogonal molecular axis coordinates for the m.r.f.'s in Table 7 for the 8 [(II), (III) and (IV)], 7 [(V) and (VI)] and 9 [(VII) and (VIII)] atoms of each substructure, so that they may be used in molecular graphics or other crystallographic or computational applications. It should be stressed that these coordinates, drawn from individual crystal structures, will not generate the mean torsion angles shown in Table 6(*a*), nor the mean geometries cited in Table 8 and discussed below.

We now consider the classifications reported in Table 6 for subsets of the individual substructures (II)–(VIII) in the context of the energy calculations of Table 4. Of particular interest are any chemical or structural features that may cause a particular fragment to adopt a higher energy conformation. The mean bond lengths and angles within (II)–(VIII) (see Table 8) are also discussed in these subsections. These data have been calculated across all observations of each substructure, it being unrealistic to generate mean values for each conformer in view of the small data sets involved. Mean values take account of the appropriate topological symmetry in each case.

Exo-unsaturated fragments [(II), (III) and (IV)]

The general dominance of TC^3 and C^1 conformers in these data sets is as expected from the energy calculations. However, the TC^4 conformer which is calculated to be almost isoenergetic with TC^3, C^1 is only prominent ($N_p = 8$) for methylenecycloheptane

Table 7. *Orthogonal coordinates referred to molecular axes for the most representative fragments of each conformational subgroup having* $N_p \geq 4$ *in Table* 6(*a*)

Data for (III) are taken from the visual classification of Table 6(*b*). For each reference code, the coordinates are ordered from 1–7 in the nomenclature of Fig. 1. The extra-annular atom is included where appropriate as atom 8 in each list.

Data set	*x*	*y*	*z*	*x*	*y*	*z*
(II)	DHYGUA (TC^3)			SAYZOH (TC^2)		
	0.00000	0.00000	0.00000	0.00000	0.00000	0.00000
	1.50358	0.00000	0.00000	1.50772	0.00000	0.00000
	2.17781	1.38807	0.00000	2.26336	1.36046	0.00000
	1.49259	2.37847	−0.95133	1.63617	2.39534	0.92283
	0.36465	3.18414	−0.28213	0.22297	2.82629	0.50687
	−0.91252	2.35684	−0.01834	−0.90945	2.06808	1.18663
	−0.68924	1.06924	0.75887	−0.71858	0.54840	1.20206
	−0.70284	−0.89600	−0.60902	−0.65071	−0.52492	−1.02679
	MIKTIN (C^1)			CELPEO (TC^4)		
	0.00000	0.00000	0.00000	0.00000	0.00000	0.00000
	1.52450	0.00000	0.00000	1.50165	0.00000	0.00000
	2.18488	1.40539	0.00000	2.18852	1.36494	0.00000
	2.19412	2.06571	1.38994	2.42940	1.96180	1.37973
	0.82107	2.31810	1.94112	1.15560	2.37842	2.13195
	0.00397	1.07563	2.29081	0.12659	1.28513	2.25029
	−0.83876	0.56049	1.12395	−0.65802	0.99222	0.94871
	−0.52682	−0.59448	−1.08300	−0.73447	−0.76002	−0.82935
(III)	FUSNEM (TC^3)			JIDHUZ (C^1)		
	0.00000	0.00000	0.00000	0.00000	0.00000	0.00000
	1.51762	0.00000	0.00000	1.55622	0.00000	0.00000
	2.06884	1.42898	0.00000	2.23573	1.40511	0.00000
	1.96689	2.15876	1.32568	2.01909	2.19661	−1.30489
	0.57419	2.32105	1.93329	0.61521	2.67560	−1.58754
	−0.03168	0.96499	2.40565	−0.32108	1.58686	−2.03477
	−0.72791	0.06980	1.35189	−0.97740	0.74304	−0.92738
	−0.61308	−0.07906	−1.03782	−0.51641	−0.67905	0.88123
	HAESTD (C^2)			FUFLAT (TC^2)		
	0.00000	0.00000	0.00000	0.00000	0.00000	0.00000
	1.51343	0.00000	0.00000	1.50442	0.00000	0.00000
	2.09341	1.44500	0.00000	2.00222	1.46619	0.00000
	1.75258	2.24283	−1.26976	1.19191	2.46682	−0.79464
	0.23614	2.52169	−1.46132	0.66534	1.96387	−2.15243
	−0.64802	1.42626	−2.09765	−0.66095	1.22887	−2.07337
	−0.73458	0.03736	−1.37888	−0.64034	−0.11910	−1.37118
	−0.59096	0.04601	1.01386	−0.66720	0.17902	0.98740
(IV)	BUVVAP (C^1)			CACBEN (TC^3)		
	0.00000	0.00000	0.00000	0.00000	0.00000	0.00000
	1.49541	0.00000	0.00000	1.50245	0.00000	0.00000
	2.14162	1.41170	0.00000	2.02605	1.41140	0.00000
	2.23837	1.95959	1.42863	1.84130	2.14993	−1.33630
	0.89844	2.21199	2.14012	0.39338	2.22905	−1.80559
	0.03181	0.98070	2.37973	−0.21095	0.91689	−2.38703
	−0.78236	0.53703	1.17157	−0.70615	−0.11662	−1.34973
	−0.53392	−0.54193	−1.03372	−0.72987	0.11417	1.02031
(V)	BUJRED (TC^1)			JAMVUI (TC^2)		
	0.00000	0.00000	0.00000	0.00000	0.00000	0.00000
	1.40522	0.00000	0.00000	1.43053	0.00000	0.00000
	2.04349	1.39395	0.00000	2.00424	1.41098	0.00000
	1.17212	2.43110	0.72810	1.55739	2.26954	1.16852
	0.07480	3.03218	−0.16051	0.06867	2.63575	1.07566
	−1.04931	2.08816	−0.58109	−0.89961	1.61508	1.63848
	−0.58084	0.74220	−1.07548	−0.57961	0.15957	1.30190
	GETKEV (C^2)			JAMVOI (C^3)		
	0.00000	0.00000	0.00000	0.00000	0.00000	0.00000
	1.40590	0.00000	0.00000	1.43224	0.00000	0.00000
	2.09921	1.31010	0.00000	1.98341	1.42837	0.00000
	1.28553	2.60102	−0.09094	1.58119	2.23441	−1.21621
	0.29929	2.76885	−1.23763	0.14151	2.73513	−1.14879
	−0.95594	1.93558	−1.14459	−1.00406	1.71858	−1.35997
	−0.74651	0.42573	−1.15047	−0.58639	0.25333	−1.29961

Table 7 (*cont.*)

Data set	*x*	*y*	*z*	*x*	*y*	*z*
(VI)	VANRAD (TC^3)			STEMON10 (C^1/TC^4)		
	0.00000	0.00000	0.00000	0.00000	0.00000	0.00000
	1.48828	0.00000	0.00000	1.55854	0.00000	0.00000
	2.03658	1.40626	0.00000	2.21872	1.29511	0.00000
	1.90804	2.15833	−1.30637	2.46882	1.78536	−1.47090
	0.50004	2.23969	−1.86485	1.24348	2.11485	−2.21095
	−0.04381	0.91608	−2.35368	0.24843	0.97435	−2.33141
	−0.70283	0.04590	−1.32346	−0.64551	0.74535	−1.14548
(VII)	JOCCOT (C^1)					
	0.00000	0.00000	0.00000			
	1.32224	0.00000	0.00000			
	2.06360	1.24093	0.00000			
	1.95490	2.02429	−1.28780			
	0.68568	2.83993	−1.49781			
	−0.59408	2.00187	−1.46013			
	−0.76150	1.28091	−0.11813			
	−0.54021	−1.07369	0.10815			
(VIII)	CAPLAC01 (C^1)					
	0.00000	0.00000	0.00000			
	1.32918	0.00000	0.00000			
	2.17969	1.20670	0.00000			
	2.07426	2.03174	1.25308			
	0.79808	2.87822	1.35857			
	−0.49710	2.07639	1.33635			
	−0.73967	1.31674	0.04476			
	−0.64028	−1.06621	−0.06508			

Table 8. *Mean bond lengths* (Å) *and valence angles* (°), *with e.s.d.'s in parentheses, for the seven-membered rings of the data sets* (II)–(VIII)

D1–D7 refer to the bonds identified by τ_1–τ_7 of Fig. 1, and A1–A7 are the valence angles having atoms 1–7 (Fig. 1) as the vertex.

	(II)	(III)	(IV)	(V)	(VI)	(VII)	(VIII)
D1	1.511 (1)	1.515 (2)	1.506 (2)	1.428 (1)	1.473 (4)	1.340 (3)	1.339 (3)
D2	1.539 (1)	1.546 (3)	1.533 (2)	1.525 (1)	1.501 (4)	1.465 (3)	1.446 (7)
D3	1.533 (1)	1.531 (2)	1.517 (3)	1.523 (1)	1.518 (3)	1.536 (6)	1.530 (5)
D4	1.532 (2)	1.529 (2)	1.523 (2)	1.532 (2)	1.513 (5)	1.554 (6)	1.534 (5)
D5	1.533 (1)	1.531 (2)	1.517 (3)	1.523 (1)	1.518 (3)	1.549 (5)	1.530 (4)
D6	1.539 (1)	1.546 (3)	1.533 (2)	1.525 (1)	1.501 (4)	1.526 (14)	1.541 (4)
D7	1.511 (1)	1.515 (2)	1.506 (2)	1.428 (1)	1.473 (4)	1.501 (3)	1.517 (4)
A1	118.7 (2)	119.6 (3)	119.4 (3)	115.9 (2)	117.5 (2)	121.3 (4)	117.8 (4)
A2	114.9 (1)	113.1 (4)	114.0 (4)	111.9 (2)	114.9 (3)	123.9 (8)	125.1 (4)
A3	114.4 (2)	114.6 (3)	115.0 (3)	114.6 (2)	115.9 (3)	113.1 (6)	113.3 (4)
A4	114.7 (2)	116.0 (2)	115.5 (3)	115.0 (2)	115.3 (4)	118.0 (7)	113.6 (3)
A5	114.7 (2)	116.0 (2)	115.5 (3)	115.0 (2)	115.3 (4)	112.6 (10)	115.2 (5)
A6	114.4 (2)	114.6 (3)	115.0 (3)	114.6 (2)	115.9 (3)	115.1 (10)	114.6 (6)
A7	114.9 (1)	113.1 (4)	114.0 (4)	111.9 (2)	114.9 (3)	115.1 (8)	112.9 (5)

(II). There are two clear TC^4 conformers for (III) and none for (IV), although the predicted global minimum for (IV) (C^1) is the major contributor with $N_p = 9$ of 16 fragments.

The most interesting feature for (II) and (III) is the presence of significant populations of higher energy TC^2 and C^2 conformers. One of the five obvious C^2 conformers of (III) has cyclopropyl fusion on bond 2 (C2—C3), thus forcing a zero τ_2 as in cycloheptane (Allen, Howard & Pitchford, 1993). The other four cases all exhibit steric overcrowding at C2 and C3. All have a quaternary C2 atom, and C2—C3 is fused to a five-membered ring which, in three cases is further fused [(XIII)], placing extra constraints on

C2. If the five-membered ring is not further fused, then C3 is also quaternary [(XIII)].

The 14 TC^2 conformers of (II) are even more distinct: ten of these contain substructure (XIV) exactly and three more are identical except that the *exo*-methylene of the fused furan ring is replaced by a methyl group. Ring *A* [(XIV)] has a variety of substituents but, in all cases where the ring *A* bonds are single, the TC^2 conformation is preserved. The γ-lactone (furanone) ring *B* is forced to be planar due to stereoelectronic effects at oxygen (Kirby, 1983) and it appears that, in combination with the ring *A* constraints, the cycloheptanone is forced to adopt a TC^2 conformation.

The mean geometries of (II)–(IV) (Table 8) are unremarkable. Intra-annular C_{sp^3}—C_{sp^3} bond lengths are typical and any differences can be ascribed to the degree of substitution of these C atoms (see *e.g.* Allen, Kennard, Watson, Brammer, Orpen & Taylor, 1987). The C_{sp^3}—C_{sp^2} distances are normal and the intra-annular angle at C1 is only slightly less than 120° in all cases.

Hetero-cycloheptanes [(V) *and* (VI)]

The lower energy TC^2, TC^3 conformations predominate for (V) (30 out of 50 examples), while the occurrence of TC^3 as the major conformer for (VI) is in agreement with our energy calculations (Table 4). The major higher energy conformers of (V) are C^2 and C^3. Six of the C^2 conformers arise from constraints imposed by small-ring fusion at C2—C3. One of the others is the only example of a free β-D-glucoheptanoside, *i.e.* one in which there is no further cyclization through adjacent oxygen substituents. The final C^2 conformer is another example of a penta-substituted ring analogous to the sugar substitution pattern. Most of the C^3 examples arise from the *trans*-isomer of the oxepano-oxepane fragment (XIV), for which the *cis*-isomer adopts a distorted TC^3 conformation.

For (VI), the smaller cluster represents a chaining in the C^1—TC^4 area of conformational space. The presence of a quaternary N^+ bonded to an increasing number of non-H atoms appears to drive the conformation towards C^1. However, the clearest examples of the C^1 conformation occur in two structures involving N lone-pair delocalization in >N—N=C— and >N—C=N— systems.

Once again, the mean bond lengths and valence angles for (V) and (VI) are as expected. The only value which is worthy of comment is the angle A1 which reaches a value of 117.5 (2)° in azepanes. This value implies a degree of N_{sp^2} involvement as might be expected from the range of conjugative substituents (*e.g.* phenyl, —C=O *etc.*) at the N atom in (VI).

Lactones and lactams [(VII) *and* VIII)]

As expected, the C^1 conformer is completely dominant for (VIII) (9 of 10 observations) and for (VIII) (all 23 fragments). The only outlier is surenolactone (Kraus, Kypke, Grimminger, Sawitzki & Schwinger, 1982), in which a TC^5 conformation is observed for an ε-lactone ring fused to a unsaturated ε-lactone ring [(VII) with a double bond at C6=C7].

The geometry of lactones and lactams has been discussed in detail by Norskov-Lauritsen, Bürgi, Hofmann & Schmidt (1985) who present mean geometry for both ε-lactones (VII) and ε-lactams (VIII). Our results agree with and extend their averages, which were taken over only four examples of (VII) and seven of (VIII).

Concluding remarks

This paper describes and illustrates a variety of methods for the mapping and classification of *exo*-unsaturated and heterocyclic seven-membered rings. The results of this survey are in broad agreement with the features of the potential energy hypersurface as calculated by force-field techniques within a novel algorithm that does not involve ring breakage. Given that these energy calculations were performed on unsubstituted parent rings for (II)–(VIII), and that most of the observations of these rings in crystal structures are heavily substituted and fused in very different ways, the qualitative agreement between theory and experiment is, perhaps, better than might have been expected. There is evidence here that, despite some relatively low energy barriers along the C/TC pseudorotation pathway, the individual rings attempt to adopt lower energy conformations even as subunits of much more complex structures. Whilst it is formally invalid to attempt to quantify conformational energy differences on the basis of population ratios observed in crystal structures (Bürgi & Dunitz, 1988), surveys of this type add to a general pool of evidence that crystal conformations do tend to map the low-energy features of the relevant potential energy hypersurface.

We would conclude that, if crystal conformations are to be used in molecular modelling or other computational applications, then the N_p-ordered classifications exemplified by Table 6 are an acceptable guide to the corresponding relative energies. One of the aims of this series of papers is to examine current methodologies for conformational classification so that, ultimately, such surveys can be carried out as a routine preliminary to any modelling experiment involving novel substructures. The current study, involving relatively small numbers of observations for each substructure, indicates that

algorithmic improvements are desirable in these cases and work to devise these improvements is in hand.

We thank Dr Olga Kennard FRS for her interest in this work and Mrs Dee Hughes for preparing Figs. 2(*a*) and 2(*b*).

References

ALLEN, F. H., DAVIES, J. E., GALLOY, J. J., JOHNSON, O., KENNARD, O., MACRAE, C. F., MITCHELL, E. M., MITCHELL, G. F., SMITH, J. M. & WATSON, D. G. (1991). *J. Chem. Inf. Comput. Sci.* **31**, 187–204.

ALLEN, F. H., DOYLE, M. J. & TAYLOR, R. (1991*a*). *Acta Cryst.* B**47**, 41–49.

ALLEN, F. H., DOYLE, M. J. & TAYLOR, R. (1991*b*). *Acta Cryst.* B**47**, 50–61.

ALLEN, F. H., GARNER, S. E., HOWARD, J. A. K. & PITCHFORD, N. A. (1994). *Acta Cryst.* B**50**, 395–404.

ALLEN, F. H., HOWARD, J. A. K. & PITCHFORD, N. A. (1993). *Acta Cryst.* B**49**, 910–928.

ALLEN, F. H., KENNARD, O., WATSON, D. G., BRAMMER, L., ORPEN, A. G. & TAYLOR, R. (1987). *J. Chem. Soc. Perkin Trans.* 2, pp. S1–S19.

ALLINGER, N. L. (1982). *Pure Appl. Chem.* **54**, 2515–2522.

ALLINGER, N. L., TRIBBLE, M. T. & MILLER, M. A. (1972). *Tetrahedron*, **28**, 1173–1190.

BOCIAN, D. F., PICKETT, H. M., ROUNDS, T. C. & STRAUSS, H. L. (1975). *J. Am. Chem. Soc.* **97**, 687–695.

BOCIAN, D. F. & STRAUSS, H. L. (1977*a*). *J. Am. Chem. Soc.* **99**, 2876–2882.

BOCIAN, D. F. & STRAUSS, H. L. (1977*b*). *J. Am. Phys.* **67**, 1071–1081.

BOCIAN, D. F. & STRAUSS, H. L. (1977*c*). *J. Am. Chem. Soc.* **99**, 2866–2876.

BOESSENKOOL, I. K. & BOEYENS, J. C. A. (1980). *J. Cryst. Mol. Struct.* **10**, 11–18.

BOEYENS, J. C. A. & EVANS, D. G. (1989). *Acta Cryst.* B**45**, 577–581.

BÜRGI, H.-B. & DUNITZ, J. D. (1988). *Acta Cryst.* B**44**, 445–448.

BURKERT, R. & ALLINGER, N. L. (1982). *Molecular Mechanics.* Monograph No. 148. Washington, DC: American Chemical Society.

Cambridge Structural Database (1992). *CSD User's Manual.* Cambridge Crystallographic Data Centre, 12 Union Road, Cambridge, England.

CHATFIELD, C. & COLLINS, A. J. (1980). *Introduction to Multivariate Analysis.* London: Chapman and Hall.

CREMER, D. & POPLE, J. A. (1975). *J. Am. Chem. Soc.* **97**, 1354–1358.

HENDRICKSON, J. B. (1967). *J. Am. Chem. Soc.* **89**, 7047–7054.

JARVIS, R. A. & PATRICK, E. A. (1973). *IEEE Trans. Comput.* **22**, 1025–1034.

KIRBY, A. J. (1983). *The Anomeric Effect and Related Stereoelectronic Effects at Oxygen.* Berlin: Springer-Verlag.

KRAUS, W., KYPKE, K., GRIMMINGER, W., SAWITZKI, G. R. & SCHWINGER, G. (1982). *Liebigs Ann. Chem.* pp. 87–93.

MORLEY, S. D., ABRAHAM, R. J., HAWORTH, I. S., JACKSON, D. E., SAUNDERS, M. R. & VINTER, J. G. (1991). *J. Comput. Aided Mol. Des.* **5**, 475–504.

MURRAY-RUST, P. & BLAND, R. (1978). *Acta Cryst.* B**34**, 2527–2533.

MURRAY-RUST, P. & RAFTERY, J. (1985*a*). *J. Mol. Graph.* **3**, 50–59.

MURRAY-RUST, P. & RAFTERY, J. (1985*b*). *J. Mol. Graph.* **3**, 60–69.

NOE, E. A. & ROBERTS, J. D. (1971). *J. Am. Chem. Soc.* **93**, 7261–7265.

NORSKOV-LAURITSEN, L., BÜRGI, H.-B., HOFMANN, P. & SCHMIDT, H. R. (1985). *Helv. Chim. Acta*, **68**, 76–82.

PICKETT, H. M. & STRAUSS, H. L. (1970). *J. Am. Chem. Soc.* **92**, 7281–7288.

Polyhedron Software (1993). Salford FTN77 Memory Manager, Polyhedron Software, Magdalene House, 98 Abingdon Road, Standlake, Witney, Oxford OX8 7AN, England.

VINTER, J. G., DAVIS, A. & SAUNDERS, M. R. (1987). *J. Comput. Aided Mol. Des.* **1**, 31–50.

Acta Cryst. (1994). B**50**, 395–404

Symmetry-Modified Conformational Mapping and Classification of the Medium Rings from Crystallographic Data. III. *endo*-Unsaturated Seven-Membered Rings

BY FRANK H. ALLEN* AND STEPHANIE E. GARNER

Cambridge Crystallographic Data Centre, 12 Union Road, Cambridge CB2 1EZ, England

AND JUDITH A. K. HOWARD* AND NIGEL A. PITCHFORD

Department of Chemistry, University of Durham, South Road, Durham DH1 3LE, England

(*Received* 12 *August* 1993; *accepted* 25 *January* 1994)

Abstract

Crystallographic results retrieved from the Cambridge Structural Database (CSD) have been used to perform systematic conformational analyses for cycloheptene, cyclohepta-1,3-diene, cyclohepta-1,4-diene and cyclohepta-1,3,5-triene. Conformational mappings based on symmetry-adapted deformation coordinates show that, with the exception of cycloheptene (for which a C^4 conformation is dominant),

* Authors for correspondence.